IEPC-95-195

Laser Interferometry for Pulsed Plasma Thruster Performance Measurement*

E.A. Cubbin† J.K. Ziemer‡ E.Y. Choueiri§ and R.G. Jahn¶
Electric Propulsion and Plasma Dynamics Laboratory
Princeton University
Princeton, New Jersey 08544

IEPC-95-195

Abstract

An optical Interferometric Proximeter System (IPS) for measuring the thrust of pulsed thrusters, in particular pulsed plasma thrusters, has been designed and developed. Unlike existing thrust stands, the IPS-based thrust stand offers the advantage of a *single* system that can yield EMI-free, high accuracy (< 3% error) thrust measurements within a very wide range of impulses (100 μN-s to above 10 N-s) covering the impulse range of all known pulsed plasma thrusters. The IPS-based thrust stand relies on measuring the dynamic response of a swinging arm using a two-sensor laser interferometer with a 10 nm position accuracy. The paper addresses the fundamentals, design, hardware implementation, data reduction and error analysis associated with the technique. The wide application of the thrust stand is demonstrated with thrust measurements of an ablative pulsed plasma thruster (APPT) and a gas-fed Magnetoplasmadynamic (MPD) thruster.

1 Introduction

The performance of many steady-state electric thrusters improves as the operating power level is increased. Due to the limited available power in most foreseeable missions, instantaneous pulsed high power provides better performance while requiring low average power levels. Pulsed plasma thrusters, such as the ablative pulsed plasma thruster (APPT), are currently the only viable high specific impulse propulsion options on small spacecraft with available power levels less than 200 W. The mass savings advantage[1, 2] pulsed plasma thrusters offer to many near-term power-limited small satellites has renewed interest in these devices and consequently in the accurate measurement of their performance. The most critical performance measurement is that of thrust.

Aside from short pulse thrusters, there is a need to study the performance of quasi-steady pulsed thrusters which are used in the laboratory as a simulation of steady-state high power thrusters that are intended for more futuristic high-power (MW-level) missions. For such thrusters the requirement is not only to measure the total impulse but also to resolve the thrust *during* the pulse in order to estimate the equivalent steady-state thrust. This is especially crucial when the current pulse used for steady-state simulation differs from a perfect rectangular pulse. This is often the case when using a real pulse forming network (PFN).

Although diagnostic methods already exist for impulse bit and instantaneous thrust measurements of various magnitudes, no *single* high-accuracy diagnostic is known to measure impulse values throughout the entire operating range of typical PPTs, and resolve the thrust of quasi-steady pulsed plasma devices. An optical interferometric proximeter system (IPS) was designed to meet these needs while providing other advantages.

In the past, impulse and instantaneous thrust measurement systems typically used either a proximeter, an accelerometer, a linear voltage differential transformer (LVDT), or a differential plate capacitance system. These devices are used to record the dy-

*Support from Air Force Office of Scientific Research and NASA Jet Propulsion Laboratory.

†Graduate Student, Department of Mechanical and Aerospace Engineering
‡Graduate Student, Department of Mechanical and Aerospace Engineering
§Chief Scientist and Lab Manager, Member AIAA
¶Professor, of Aerospace Sciences, Fellow AIAA

namic response of a particular location on the thrust stand to the firing of the thruster.

The proximeter is a device that reflects radio frequency signals off of a metal target which is attached to the thrust stand[3] to measure position. Experience with the proximeter shows that it can suffer from electromagnetic interference (EMI) problems[4]. This renders the device useless to resolve the impulse *during* the plasma discharge associated with many thrusters and can also induce residual signal corruption after the pulse.

An accelerometer is limited by typical rise times of >1 μs. Typical Ablative Pulsed Plasma Thruster (APPT) pulse are on the order of 1 μs[5] and thus renders the accelerometer useless for this type of measurement. Since the accelerometer must be located on the thrust stand it is also susceptible to EMI.

The LVDT has demonstrated position resolution of 500 nm for an impulse measurement system and is adequate for some impulsive measurements[6]. However, resolving thrust during pulses for many plasma thrusters demands <30 nm spatial resolution for accurate second derivative calculations needed for instantaneous thrust calculations. EMI may also be a problem with the LVDT during a pulse.

The differential plate capacitance system has demonstrated 25 nm spatial resolution[7]. This is quite adequate for impulsive measurements but not for resolving thrust due to potential EMI problems and the limited resolution.

This paper presents the IPS as a single diagnostic instrument capable of measuring impulse bits and instantaneous thrust for all plasma thrusters of common interest. The IPS utilizes basic principles of optical interference to record the dynamic repose of the thrust stand to the firing of a thruster. A laser beam is reflected off a corner cube which is attached to the thrust stand. This laser beam is then interfered with a reference beam and the resultant light intensity is measured using photo-diodes. The light intensity information can be unfolded to give the dynamic position history of the corner cube. From this dynamic position history the thruster performance is determined. The following methodology applies to a wide assortment of thrusters and thrust stand arrangements. The general method will be described and then specified to two examples.

2 Thrust Measurement Fundamentals

2.1 Thrust Stand Dynamics

Thrust stand systems can be treated like a "black box." The input to the system is the applied thrust and the response of the system can be observed from many locations within the thrust stand system. The exact dynamic response of each observation point on a thrust stand to a given thrust input can, in general, be complex. Fortunately, in many cases the thrust stand can be modeled with a high degree of accuracy as a damped spring-mass system. If the motion of the observation point is characterized by x, and the effective natural frequency, damping constant, and mass are $\omega_{n,eff}$, ζ_{eff}, and m_{eff} respectively, the applied impulse bit (I_{bit}) will force the response[8]

$$x(t) = e^{-\zeta_{eff}\omega_{n,eff}t}\frac{I_{bit}/m_{eff}}{\omega_{n,eff}\sqrt{1-\zeta^2}} \sin\left(\sqrt{1-\zeta^2}\omega_{n,eff}t\right). \quad (1)$$

The duration of the impulse must be much less then the natural period of the observation point for equation 1 to be valid. In many of such cases, measurements can be made on time scales where the effects of the spring and damper are negligible. In the absence of a spring and damper, this model leads to the simple momentum equation,

$$I_{bit} = m_{eff}\Delta\dot{x}, \quad (2)$$

where $\Delta\dot{x}$ is the change in velocity of the observation point from before to after the impulse. Likewise, for a free body, Newton's equation,

$$\ddot{x} = T/m_{eff}, \quad (3)$$

governs the dynamics where $\ddot{x}$ is the acceleration of the observation point and T is the instantaneous thrust. In order to compute I_{bit} or T, the effective parameters must be determined. This can be done by applying a known impulse to the system and observing the dynamic response. This is discussed in section 3. Whether the appropriate model is this simple or not, the position coordinate provides the dynamic response of the system to an excitation. The IPS was designed around this idea and can provide continuous position data with accuracy as high as 10 nm.

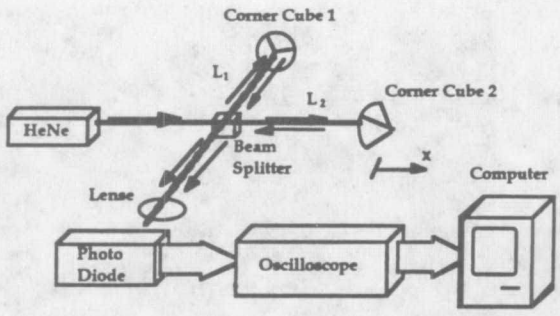

Figure 1: IPS schematic

2.2 Position Measurement with the IPS

The IPS is based on the Michelson interferometer[9]. Figure 1 shows a schematic of the IPS. Light emitted from the laser source is split into two beams at the beam splitter. One beam then traverses the path L_1 while the other traverses path L_2. At the end of each path is a corner cube. Corner cubes reflect light such that the incident ray and the reflected ray are parallel regardless of the incidence angle. This considerably simplifies the alignment process of an interferometric system. The two beams are reflected back to the beam splitter and passed through a lens to the diode sensors. The diode sensor output signals are recorded and sent to a computer. The projected pattern of light is a multiple fringe pattern in general. If the beams are precisely aligned then there would be a uniform intensity cross section of light incident on the diode array. The phase of the electric field of a light wave has a sinusoidal spatial dependence. When the path lengths traversed by the two beams differ by a non-integer multiple of the wavelength of the laser light (λ) there is a phase angle difference (ϕ) between them when they are reunited. Superposition of these two waves yields constructive or destructive interference. If only corner cube 2 is allowed to move, then it can be shown (see Appendix) that the intensity of light (I) at a particular location on the diode array is related to the relative position (x) of corner cube 2 by[10]

$$I(t) = \frac{I_{max}}{2}\left[1 + \cos\left(\frac{4\pi x(t)}{\lambda}\right)\right]. \qquad (4)$$

Eqn. 4 shows that if $\dot{x}$ is constant, $I(t)$ will appear as a continuous cosine function with a constant frequency (ω_{IPS}) of

$$\omega_{IPS} = \frac{4\pi\dot{x}}{\lambda}. \qquad (5)$$

The frequency of the IPS output signal increases with the velocity of the observation point. For instance, by keeping corner cube 1 inertially still and placing corner cube 2 at a location on the thrust stand, the inertial motion of that location can be measured. Relative motion of two locations on the thrust stand can also be measured. In either case, the dynamic motion of the thrust stand can be observed.

2.2.1 Double Diode Sensor Method

There are two disadvantages to using a single diode sensor to monitor position. From Eqn. 4, the position can be obtained by properly taking the arccosine of the intensity signal. The first disadvantage of this technique is that the sensitivity of the cosine function goes to zero at maximum and minimum light intensities. In other words (again consider Eqn. 4) if the intensity is at maximum when a change in x occurs, the result is a relatively small change in the light intensity. Compare this to the case when the present light intensity level is in between a maximum and a minimum in which case the resulting change of light intensity is much larger and quite linear.

A second disadvantage to using a single diode sensor to monitor position is that direction reversals can sometimes go undetected. When x is a half integer multiple of λ, I is at a maximum. No matter which way x moves from this point in time, the intensity will diminish, thus direction ambiguity is demonstrated. Both of these disadvantages can be eliminated by using a double diode sensor.

In order to use the double diode sensor the interference pattern at the diode sensors should not be uniform. This can be achieved by several different methods. For example, offsetting the two interfering beams before they reach an expanding lens will result in fringes similar to those in Younge's double-slit experiment[9]. In this case, as x changes, two given locations within the fringe pattern will change intensity with frequency ω_{IPS} but these resultant cosine curves will be out of phase. By selecting two points within the fringe pattern that are 90 degrees out of phase, there is always one diode sensor output signal in the sensitive region of the cosine function. One way to unfold this double sensor information is to use a scheme known as quadrature. Normalizing the two outputs and plotting one signal versus the other will

produce data which falls on the unit circle. In this case the angle is proportional to x. An algorithm can be written which properly takes the arctangent of the data and gives the position versus time. One cycle around the unit circle corresponds to $\lambda/2$ m. The algorithm must be able to handle many cycles around the circle as well as direction reversals. This technique was used in several experiments and the results are in section 4 and 5.

2.3 Measuring Effective Parameters

Once two locations have been chosen for the relative x measurement, the effective parameters (i.e. m_{eff}, ζ_{eff}, $\omega_{n,eff}$) must be determined. This process is synonymous with calibrating the IPS. A known impulse must be given to the thrust stand while the response is recorded by the IPS. The impulse must be applied at the same location as the force which is applied during an actual firing of the thruster. A commercially available force transducer provides a simple way of applying a measurable impulse. The thruster must be struck with the force transducer while the force transducer output voltage is being recorded. Integrating the force with respect to time yields total impulse. The IPS should record the dynamic response of the thrust stand to the impulse. From this information, all of the effective parameters can be determined by fitting the thrust stand mathematical model to the data. In the case of a damped spring-mass model initially at rest, the IPS position data must be fit to Eqn. 1 using the measured total impulse for I_{bit}.

3 Experimental Setup

The following experiments were performed in the Pulsed High-Power Performance facility (PHPP) at EPPDyL.

3.1 Vacuum Facility

The vacuum vessel of the PHPP facility is a 2 m diameter, 5 m long fiberglass tank with eight optical access ports. A vacuum level on the order of 10^{-5} torr is maintained by a set of two 1.3 m diffusion pumps each with a pumping capacity of 95 m^3/s. The diffusion pumps are backed by a roots blower (1340 cfm) and two mechanical pumps (150 cfm).

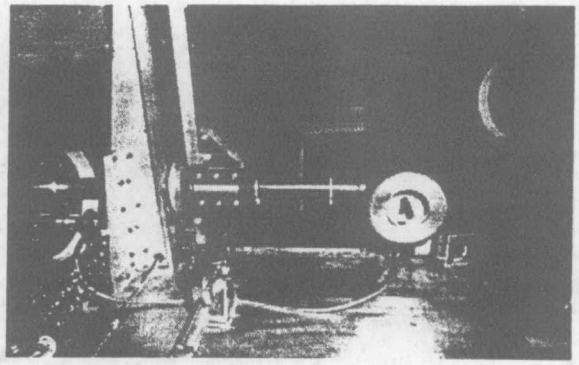

Figure 2: The gas-fed MPD thruster and thrust stand

3.2 Power Supply

The power supply for the PHPP facility consists of a 20-station 12.8 mfarad L-C pulse forming network (PFN) which can be adjusted to produce current pulses ranging from 0.5 to 2 msecs and current levels up to 50 kA. This power supply is used for the gas-fed MPD discussed in section 4. The APPT discussed in section 5 has an internal PFN and requires an external 15-30 volt unregulated 30 watt power supply.

3.3 Thrust Stand

The specimen thruster is mounted on a swinging arm thrust stand. Figure 2 shows a gas-fed coaxial MPD thruster attached to the arm. The thrust arm is mounted with two flexural pivots. They are series 6016 Bendix Free-Flex Pivots[11] each with a torsional spring constant of 0.73 N-m/rad. The vertical axis of rotation of the arm can be adjusted to incorporate the force of gravity. The force of gravity can be added or subtracted from the restoring force of the flexural pivots to influence the natural period of the arm. Typical natural periods of the arm are 1-10 seconds. The thrust stand is fully described in Ref. [12] and is a modified version of a microthrust stand built by Fairchild Republic[13]. To reduce random mechanical perturbations to the thrust stand system, the entire thrust stand table was mechanically isolated from the tank. This was done by hanging it by 9 carbon steel 1.5 inch outer diameter springs. The thrust stand mass is approximately 200 kg and the final natural period of the suspended thrust stand table was approximately 2 Hz in all directions.

3.4 IPS

At the thruster end of the tank the IPS table top was mounted at the optical access window. Figure 3 is a layout of the IPS used at the PHPP facility. One corner cube is attached to the thrust stand table and the other to the thruster. A 1 mW Helium-Neon laser was used for which λ=632.8 nm. Both the beam splitter and the right angle prism were mounted on two adjoined aluminum blocks with separate pitch angle adjustment. Also the beam splitter and right angle prism can each slide sideways to match the horizontal separation of the corner cubes. Both of these adjustments are made until both beams are coincident at the adjustable mirror. The mirror is then used to direct the beams to the diode sensors. Between the mirror and the diodes are a lens and a filter. The lens is a cylindrical lens of focal length 1 cm. This expands the beams in one dimension and facilitates the production of multiple fringes while keeping the intensity of light which is incident on the diodes at a maximum. Finally there is a 3 nm bandwidth filter at wavelength 632.8 nm. This prevents virtually all of the stray light from the surroundings from reaching the diode sensors, including light from the plasma discharge. The diode sensors are FDS100 Silicon Photodiodes from Thorlabs Inc. They have a rise time of 10 ns, an active area of 13.7 mm^2, and a spectral response of 350-1100 nm.

3.5 Calibrating Pendulum with Force Transducer Setup

A 30 cm long 0.5 kg steel rod was used as a pendulum. See figure 4. The rod pivots on a teflon pin which was fixed to an aluminum stand. This stand was mounted inside of the vacuum tank in front of the thruster. An electromagnet was also mounted on the pendulum stand so that the pendulum could be cocked and then released remotely. Care must be taken to align the pendulum so that the force is delivered along the thrust axis. See section 6.2 for a quantification of this alignment error.

The force transducer used was a model 208A02 Force Transducer from Piezotronics. The operating range is from 0-400 N. A vertical static load was applied to the force transducer to calibrate it in a range of 0-13 N. The resultant calibration constant was found to be 87.6±0.6 N/V. The output signal is recorded during an impact on a Nicolet 320 Digital oscilloscope and then analyzed on a computer. The data was digitally integrated to obtain a value for I_{bit}. See section 6.2 for a quantification of this error.

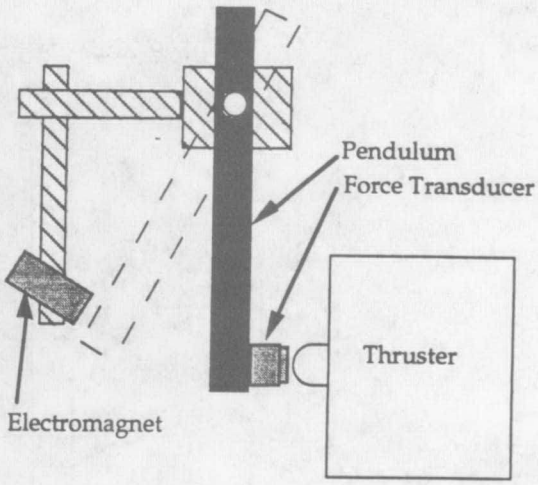

Figure 4: Pendulum for m_{eff} calibration

4 Experimental Results Using the IPS on the Pulsed Gas-fed MPD

This section describes the use of the IPS to resolve the acceleration and measure I_{bit} for the a benchmark configuration coaxial gas-fed MPD thruster. This thruster has a 12.7 cm diameter anode with a 10 cm long hemispherically tipped, 1.9 cm diameter cathode. This thruster has a 5 cm deep chamber and an anode inner radius of 5.1 cm. Propellant injection is at the back plate of the chamber. Argon at 6 g/s was used. For one pulse of the thruster, the mass flow lasts for approximately 20 ms during which is a 1.5 ms current pulse of approximately 15 kA. The self-induced magnetic field accelerates the plasma out of the discharge chamber. The operating voltage is a nominal 100 volts. The experimental equipment use for this experiment is described in section 3.

The most convenient model of the thrust stand system to use with the pulsed gas-fed MPD thruster is the free-mass model. In this case Eqn. 2 is employed and only m_{eff} needs to be determined.

The IPS was configured as shown in figure 3. The pendulum stand (see section 3 for details) was placed in front of the MPD thruster so that the force transducer would strike the tip of the cathode. Figure 5 shows the measured force and the calculated total impulse. See figure 6 for the double sensor IPS response to the impact test. This sensor data was unfolded to produce position information and is shown

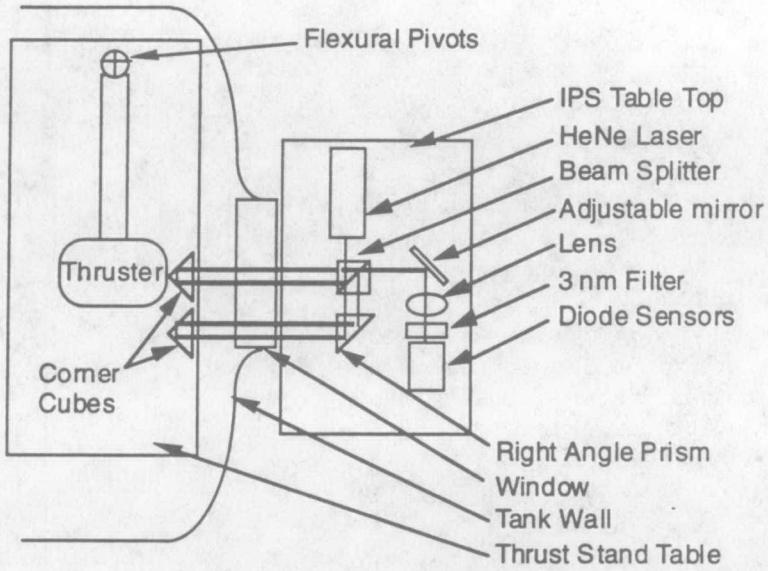

Figure 3: IPS layout at the PHPP facility

in figure 7. The natural period of the thrust stand is approximately 1 second. Therefore on time scales much shorter then 1 second, the effects of the effective spring and damping are negligible. In this case m_{eff} is found from Eqn. 2, the impulse delivered was 75.1 mN-s and thus

$$m_{eff} = \frac{I_{bit}}{\Delta \dot{x}} = \frac{75.1 \text{ mN-s}}{4.78 \text{ mm/s}} = 15.71 \pm 0.27 \text{ kg}. \quad (6)$$

With the IPS calibrated for this thrust stand arrangement, the pulsed gas-fed MPD was fired and the IPS response was once again recorded. A slope change of 5.79 mm/s was recorded. From Eqn. 2 and m_{eff}, the delivered impulse is

$$I_{bit} = 15.71\ kg \times 5.79 \text{ mm/s} = 0.091 \pm mbox 0.0016\ N-s. \quad (7)$$

4.1 Time Resolved Thrust

Time resolved position data is also of interest with the pulsed gas-fed MPD thruster. Eqn. 3 shows that if the free-mass model is accurate then only $\ddot{x}$ is needed for determining instantaneous thrust. The position data obtained by the IPS has 10 nm resolution (see section 6.1.2) and the total displacement of the thruster during the pulse is 5-10 microns. The IPS proved immune to the EMI and is shown in figure 8. The IPS position data in figure 9 should be compared to the proximeter signal shown for the same

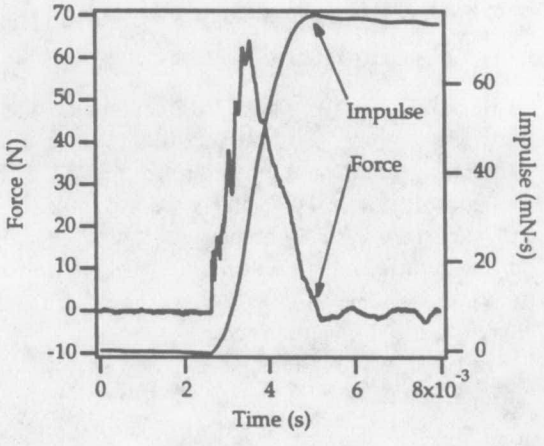

Figure 5: Force delivered by pendulum and integrated force for total impulse

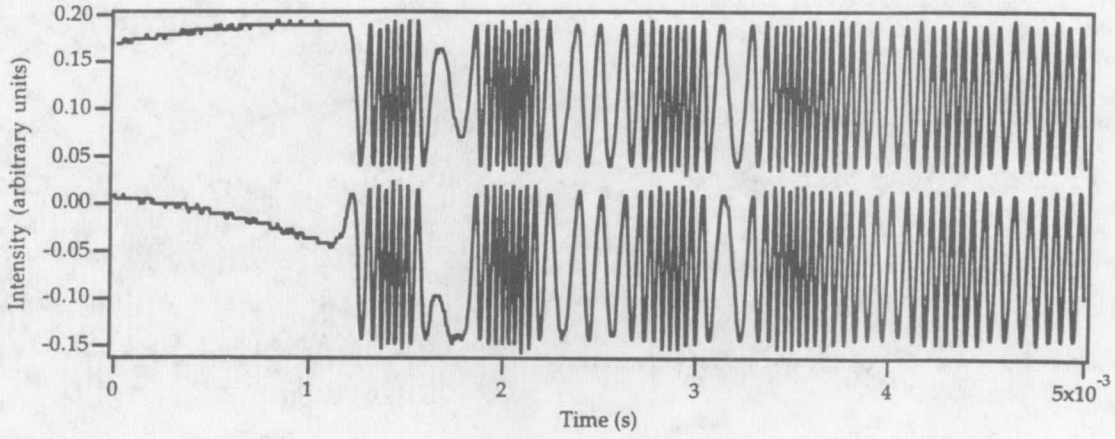

Figure 6: Double IPS output during pendulum impact

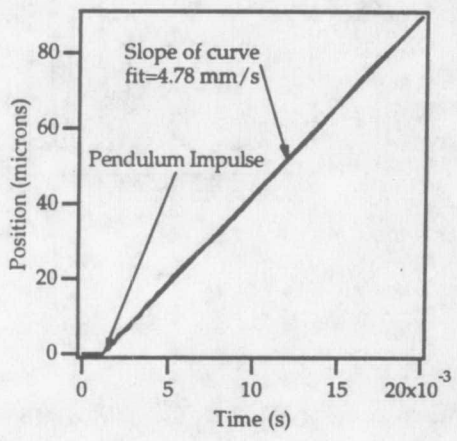

Figure 7: IPS position measurement after pendulum impact

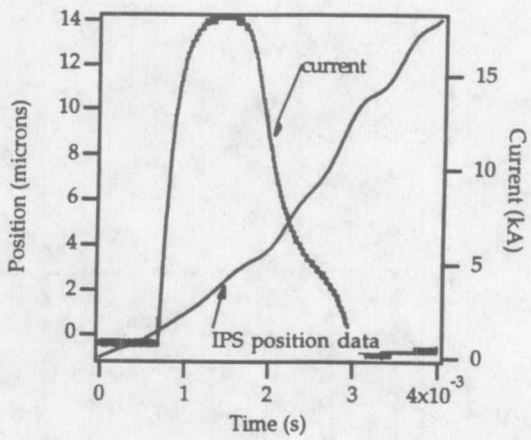

Figure 9: IPS position data during an MPD pulse

pulse in figure 9. The IPS successfully recorded the dynamic response of the pulsed MPD during the current pulse.

By differentiating x twice, $\ddot{x}$ is obtained and is shown in figure 11. The acceleration error is 2% and is discussed in section 6.3.3. The $\ddot{x}$ data reveals information about the validity of the free-mass model. The actual acceleration of the thruster fluctuates. This is typically due to structural vibrations within the thruster. Solutions to this problem include stiffening the thruster and the thrust arm[14]. The goal of this experiment was to demonstrate the capability of the IPS to resolve acceleration and this was accomplished. The stiffening of the thruster is

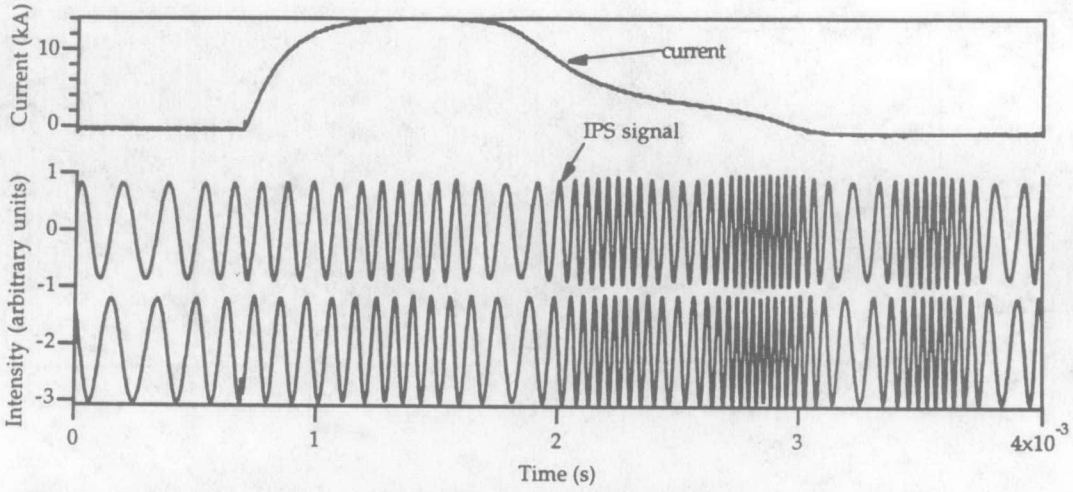

Figure 8: Double IPS output during a gas-fed MPD pulse

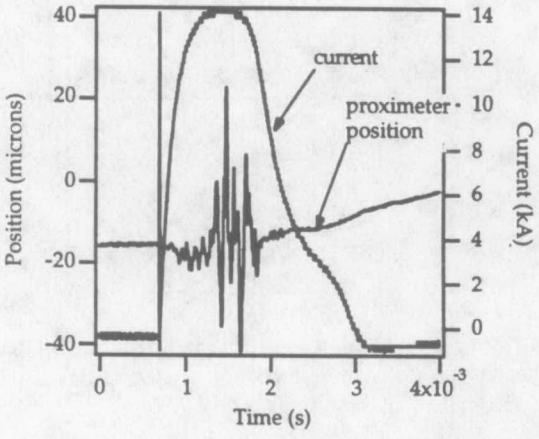

Figure 10: Proximeter position data during an MPD pulse

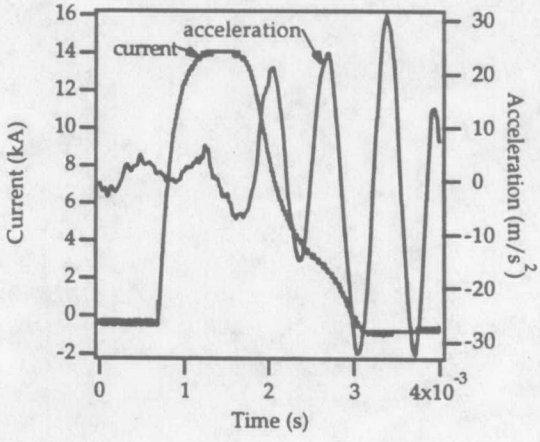

Figure 11: IPS $\ddot{x}$ after smoothing position

required to resolve the thrust of this MPD thruster.

5 Experimental Results Using the IPS with the APPT

The APPT used for this experiment is the Lincoln Experimental Satellite thruster (LES-8/9). The APPT has a mass of 6.6 kg and has a total impulse capability of 7320 N-s[5]. The impulse bit is 300 μN-s and the specific impulse is 1000 s. The PFN is internal and requires an external 25-150 watt power

supply to charge the main 17 μF oil-filled capacitor. The pulse lasts for 2-5 μs and can pulse at a maximum of 2 Hz. The discharge occurs across the surface of a Teflon fuel bar and ablates approximately 28.5 μg of propellant. There are two nozzles canted at 30 degrees to the thruster axis of symmetry. For these experiments only one nozzle was fired. The APPT was mounted on the thrust stand such that the nozzle was perpendicular to the thrust arm.

The APPT provides a much smaller impulse then the pulsed gas-fed MPD. The nominal value is 0.3 mN-s. On short time scales, the free-mass model for impulse bit calculations is always valid. However, it may be that the background noise disallows accurate $\dot{x}$ measurements to be made. In this case the second alternative is to observe longer time scales and model the system with more complexity. In the case of a damped spring-mass system Eqn. 1 describes the dynamic response. Using the force transducer method demonstrated in section 4 the effective mass can be determined. An insert was made to fit into the nozzle. The calibration pendulum struck the center of the insert. In a manner identical to that used in determining m_{eff} for the pulsed gas-fed MPD, m_{eff} was determined for the APPT thrust arm configurations with the IPS. The result was m_{eff} =12.16 kg. The IPS configuration for the APPT experiments was also as shown in figure 3. For small damping, the approximate Δx for this system is

$$\Delta x = \frac{2I_{bit}}{\omega_{n,eff} m_{eff}}. \tag{8}$$

Therefore, restoring forces on the thrust arm were minimized such that the the natural frequency was maximized and the resultant signal-to-noise ratio for position was 60:1 at maximum deflection. Section 6 discusses this quantitatively. Once the effective mass is known the position data from a damped spring-mass system can be fit to the model unambiguously. Eqn. 1 requires ζ_{eff}, $\omega_{n,eff}$, and I_{bit} for a fit. Figure 12 shows the unfolded double IPS sensor position data. The corresponding fit values are ζ_{eff} =0.0326, $\omega_{n,eff}$ =1.279 rad/s, and I_{bit} =0.243 mN-s. The uncertainty on I_{bit} was found to be $\pm$0.006 mN-s.

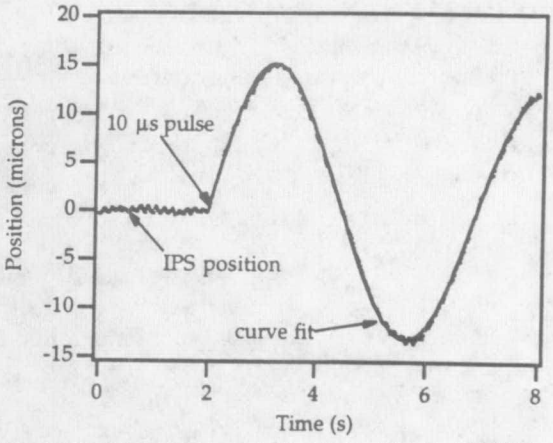

Figure 12: IPS position data with curve fit

6 Error Analysis

This section presents an error analysis for the different IPS measurements. First the IPS raw measurement error of 10 nm is experimentally determined. Then the background mechanical perturbations to the system are considered in an error analysis of the impulse bits reported above. Each final impulse value was comprised of a m_{eff} measurement and a value from a curve fit. The m_{eff} error will be determined from the accuracy of the force transducer and the estimated experimental error of alignment, and the error associated with the curve fit values will be estimated from a statistical approach, again considering the background mechanical noise.

6.1 IPS Spatial Resolution

The simplest way to quantify the position error inherent in the IPS is to perform the following experiment. The ips is set up as if to record a typical thruster pulse, as shown in figure 3. Then the right angle prism and the beam splitter are adjusted such as to aim both beams into the same corner cube. The IPS output at this point corresponds to the random noise generated within the IPS. This is the spatial resolution of the device. Before attempting this measurement, the IPS table top vibration should be considered.

6.1.1 IPS Table Top Vibrational Effects on IPS Spatial Resolution

The IPS table top will vibrate in general. The only translational motion of the table that will effect the two path lengths within the IPS is motion along the direction of the path. If both of the beams traveling into and out of the tank are parallel, this type of IPS table top motion will go unnoticed since it will

effect both path lengths in the same way. However, if the beams are not parallel, the projection of the IPS table top motion onto each path length can be different. For instance, if one beam is coincident with the motion of the IPS table top while the other differs by an angle θ, the induced path length difference ΔL becomes

$$\Delta L = \Delta x \frac{\theta^2}{2}. \quad (9)$$

It is typically quite easy to keep the IPS table top localized to 10 μm. By maintaining an angular alignment of 1 degree, the corresponding random error would equal 1.5 nm.

6.1.2 Experimental Measurement of IPS Spatial Resolution

The experiment described in section 6.1 was performed just before the pulsed thruster experiments were performed. Figure 13 begins with everything at rest. After approximately 1 s, the right angle prism was perturbed to identify the peak levels. After the peak levels are noted, the vibrating motion can be quantified. Figure 14 presents typical IPS position measurement noise. The standard deviation of this noise is 10 nm and this finally quantifies the IPS accuracy.

6.2 Error in m_{eff} measurement

The calibration constant for the force transducer was determined by applying static loads to the load cell and measuring the voltage output. Within the operating range of this experiment, the calibration constant was repeatable to within 0.7% of 87.2 N/V. The integration was done numerically on a computer. The zero level was taken as the average value before the impact (see figure 5). This value varied much less then 1% of the peak signal strength and was negligible. The integration can be done to an accuracy of 1%.

A last source of error is the alignment of the pendulum such that it strikes along the thrust axis. If an alignment of 3 degrees is maintained, the error incurred is 0.1%. The pendulum was aligned to this tolerance so the incurred error was negligible. The calculated I_{bit} for the pulsed gas-fed MPD is linearly depended on m_{eff} (see Eqn. 7) . Summing the errors identified in this section yields a 1.7% error for the m_{eff} measurement. Repetitive measurements of this value can be used to establish a distribution and statistically eliminate some uncertainty due to experimental error.

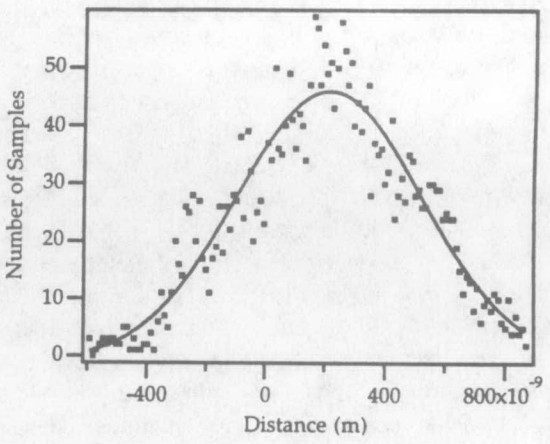

Figure 15: Scatter of data about damped spring-mass curve fit for the APPT

6.3 Error in Curve Fitted Values

6.3.1 Line Fit for Velocity

All of the curve fit data was performed using the software package called Igor Pro by WaveMetrics. In the case of the pulsed gas-fed MPD I_{bit} calculation, $\dot{x}$ was found using a line fit to the position data after the pulse. If the scatter of the data around the fit is considered noise then a standard deviation value can be computed for the slope. Igor Pro reports this computed value as 0.1% of the slope.

6.3.2 Damped Spring-Mass Equation Fit

Igor Pro reports a 0.1% standard deviation on the estimate of $\dot{x}(0)$ for Eqn. 1 fit to the IPS position data for the APPT. The scatter of data about the curve fit can be plotted in a histogram to note the noise present in the system. Figure 15 shows a gausian fit to the distribution for a reference. There is approximately a 250 nm standard deviation on the distribution as well as an offset. This offset is believed to be caused by the zero level chosen for the curve fit data. The present method is to use the average position during the 2 seconds prior to the pulse. Combining this 0.1% standard deviation with the 1.7% error of the effective mass error yields approximately 1.8% error on the APPT impulse.

6.3.3 Error for Time Resolved $\ddot{x}$

The position information obtained during the pulse of a thruster can be differentiated twice for actual ac-

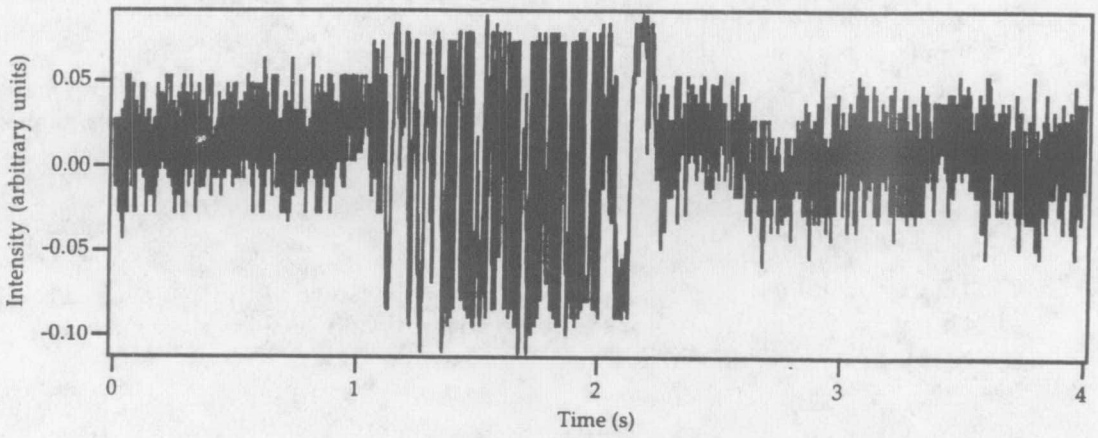

Figure 13: Background random noise signal from IPS

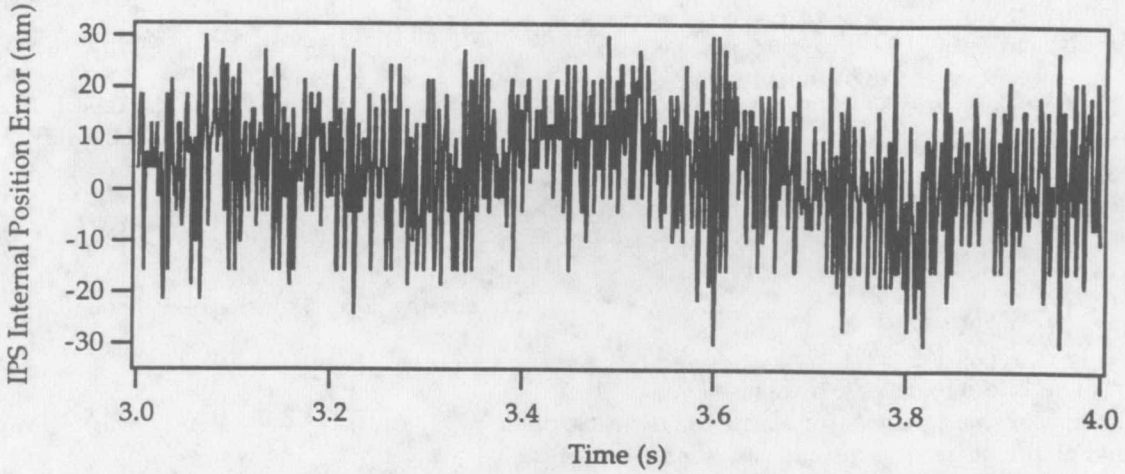

Figure 14: Position Noise; Standard Deviation is $\sigma = 10\ nm$

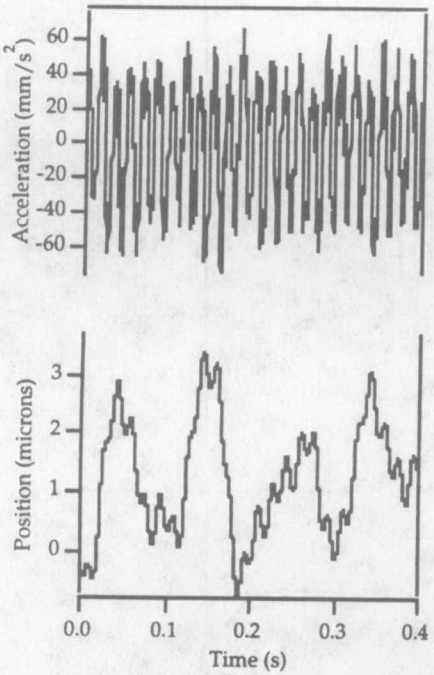

Figure 16: Background noise measured by IPS for pulsed gas-fed MPD Configuration

celeration information. It is necessary to first quantify the background noise in this acceleration measurement. Figure 16 contains a sample of the background position data taken when the thruster is not firing. By differentiating this data twice, the background acceleration can be quantified. Figure 16 shows the results. The maximum background acceleration appears to be 0.06 m/s^2. The steady state thrust for the benchmark MPD thruster is approximately 3 m/s^2[14]. The background noise is thus 2%.

7 Conclusions

An optical Interferometric Proximeter System (IPS) for measuring the thrust of pulsed thrusters, in particular pulsed plasma thrusters, has been designed and developed. The IPS has demonstrated the ability to accurately measure pulsed thruster performance for thrusters in the range of 1×10^{-4} N-s and 0.1 N-s nominal impulse values to an accuracy of <3%. The measured APPT impulse bit was 0.243±0.0044 mN-s and the measured pulsed gas-fed MPD impulse bit was 0.091±0.0016 N-s.

8 Appendix

The electric field (E_1) at a given location within a laser beam varies in time at the frequency (ω) of the laser. The magnitude of this electric field can be described by

$$E_1 = E_0 \sin(\omega t). \tag{10}$$

A second beam from the same source which traversed a different path in space and arrives at the same given location will produce an electric field (E_2) given by

$$E_2 = E_0 \sin(\omega t + \phi). \tag{11}$$

The phase of the electric field of each beam varies sinusoidally along the beam path. The difference in phase at the given location is related to L_1, L_2 and λ by

$$\phi = \frac{2\pi}{\lambda}(L_2 - L_1). \tag{12}$$

Adding these two electric fields at their meeting point gives an equation for the total electric field strength (E_{total}).

$$E_{total} = E_1 + E_2 = 2E_o \cos\frac{\phi}{2} \sin\left(\omega t + \frac{\phi}{2}\right) \tag{13}$$

The intensity of light (I) which is measured at a particular location within the fringe pattern by the photo diode, is related to the electric field strength by

$$I = \frac{E_{total}^2}{2\mu_0 c}. \tag{14}$$

Since the frequency of the laser light(ω) is $\sim 5 \times 10^{14}$ Hz, the time average light intensity (I_{ave}) will be the measured value due to the relatively slow frequency response of the diode ($\sim$ 100 KHz). The time average of Eqn. 13 becomes

$$I_{ave} = \frac{2E_0^2}{\mu_0 c}\left(\frac{1}{2}\right)\cos^2\left(\frac{\phi}{2}\right). \tag{15}$$

Simplifying Eqn. 15 using a trigonometric identity yields

$$I_{ave} = \frac{E_0^2}{2\mu_0 c}\left[1 + \cos\left(\frac{2\pi}{\lambda}(L_2 - L_1)\right)\right]. \tag{16}$$

By normalizing Eqn. 16 to the maximum observed intensity of the light (I_{max}), Eqn. 16 becomes

$$I_{ave} = \frac{I_{max}}{2}\left[1 + \cos\left(\frac{2\pi}{\lambda}(L_2 - L_1)\right)\right] \tag{17}$$

A change in the relative position in the x dimension of corner cube 1 with respect to corner cube 2 of δx

will result in a path length change of $2\delta x$ because the light travels both to and from the corner cubes. The final dependence of the light intensity on the relative position of the corner cubes is

$$I_{ave} = \frac{I_{max}}{2}\left[1 + \cos\left(\frac{4\pi(x)}{\lambda}\right)\right]. \qquad (18)$$

References

[1] R.M. Myers and S.R. Oleson. Small satellite electric propulsion options. In *29th Intersociety Energy Conversion Engineering Conference*, Monterey, California, August 7-11 1994. AIAA 94-4137.

[2] E.Y. Choueiri. A system optimization model for the application of ablative pulsed plasma thrusters to stationkeeping missions. In *30th Joint Propulsion Conference*, Indianapolis, Indiana, June 27-29 1994. AIAA 94-3392.

[3] Research activities at the electric propulsion and plasma dynamics laboratory (eppdyl). Technical/Ordering Information L5001, Bently Nevada Corporation, April 1990.

[4] Research activities at the electric propulsion and plasma dynamics laboratory (eppdyl). Progress Report EPPDyL-TR-94F, Princeton University, June-December 1994.

[5] R.J. Vondra and K.I. Thomassen. Flight qualified pulsed electric thruster for satellite control. *Journal of Spacecraft and Rockets*, 1974. Vol. 11, No 9.

[6] T.W. Haag. Ppt thrust stand. In *31st Joint Propulsion Conference and Exhibit*, San Diego, California, July 1995. AIAA 95-2917.

[7] Design and development of a micropound extended range thrust stand (merts). Technical Report NASA TN D-7029, August 1971.

[8] W.T. Thomson. *Theory of Vibrations With Applications*. Prentice-Hall, 1993.

[9] G.R Fowles. *Introduction to Modern Optics*. Dover Publications, 1989.

[10] R.A. Serway. *Physics for Scientists and Engineers*. Saunders College Publishing, 1990.

[11] Free flex flexural pivot engineering data. Technical Report 00U-6-681D, The Bendix Corporation-Fluid Power Division, March 1972.

[12] R.G. Jahn, K.E. Clark, and S.J. Leete. Inductive storage for quasi-steady magnetoplasmadynamic (MPD) thrusters. Progress Report 1405c, Princeton University, April-July 1979.

[13] Operating instructions for plasma engine microthruster stand. Technical Report RAC 2392-1, PCD-TR-65-1, Republic Aviation Corporation, January 1965.

[14] J.M. Berg, A.J. Kelly, and R.G. Jahn. Direct measurement of mpd thrust. In *17th International Electric Propulsion Conference*, Tokyo, June 27-29 1984. IEPC 84-30.